DOI: 10.1002/adem.200600152

Metallurgical Aspects of Casting High-Manganese Steel Grades**

By G. Gigacher,[+] R. Pierer, J. Wiener and C. Bernhard*

The possibility of using new, high-strength steels with an attractive forming behaviour (e.g. induced plasticity steels) in automotive manufacturing, offers a significant potential for improvement in the area of reducing the weight while simultaneously increasing crash safety. Induced plasticity steels not only possess high strength but also excellent elongation properties and high energy absorption capacities due to the TRIP and TWIP effects, Table 1.[1–4] This profile of mechanical properties is of great interest for crash-relevant automotive components.

Common TWIP steel concepts are based on high Mn and Al contents, which are known to cause various problems during steelmaking. The search for suitable primary and secondary steelmaking processes, and the feasibility of casting these steel grades on conventional continuous casting machines, is the focus of ongoing research. The aim of the work presented here is to provide a basis for decisions on the subsequent development of the industrial production of high-Mn and -Al steels.

At the very beginning, the following potential difficulties for the continuous casting of high-Mn, high-Al steels were identified:[5]

- high-temperature strength: is expected to be extremely high for these steels, and thus may be a problem for the strand guiding and soft reduction system in casting machines;
- hot tearing: the wide brittle-temperature range during the solidification of high-Mn and -Al steels indicates a high crack susceptibility;
- segregation at the micro- and macroscopic levels: possible formation of banded structures, resulting in difficulties during further processing;
- non-metallic inclusions: the possible interaction between precipitates and mechanical properties means that steel cleanliness levels (secondary metallurgy) should be defined;
- scale formation: partial oxidation plays a role in the formation of surface cracks in the casting and rolling process.

This list does not consider necessary process adjustments, such as the development of suitable mold powders for high-Al steels.

The work presented here is concerned with the high-temperature mechanical properties of an high strength structural steel (HSSS) steel and the high-Mn, high-Al steel X50MnAl 25 1 in comparison to common ultra low carbon (ULC) and electrical sheet (ES) steels, the latter both known not to cause many problems during the continuous casting process.

Methodology

The high-temperature mechanical properties and the crack susceptibility were analyzed using the SSCT (submerged split-chill tensile) method. The principle of this testing method is described in detail elsewhere.[6–8] The SSCT test was developed to simulate the shell straining during the continuous casting process. A steel cylinder, split in two halves, is submerged in a liquid steel melt inside an induction fur-

[*] *Dr. R. Pierer, Dr. J. Wiener, Dr. C. Bernhard, Dr. G. Gigacher*[+]
Christian-Doppler Laboratory for Metallurgical Fundamentals of Continuous Casting Processes
Department of Metallurgy
Montanuniversität Leoben, Austria

[+] *now with Boehler Edelstahl GmbH, Kapfenberg, Austria*
E-mail: Guenter.Gigacher@bohler-edelstahl.at

[**] *The authors gratefully acknowledge the financial support of this work by voestalpine Stahl GmbH and the Christian Doppler Research Association.*

Table 1. Composition of selected steel grades for automotive purposes with mechanical properties, RA-TRIP: retained austenite – transformation induced plasticity, TWIP: twinning induced plasticity, DDG: conventional deep drawing steel grade. [1–4]

	Composition				Mechanical Properties		
Steel grade	Cwt.- %	Mnwt.-%	Alwt.-%	Siwt.-%	Tensile StrengthMPa	Fracture elongation %	Energy absorption capacity J/mm
RA-TRIP	0.1–0.4	1–2	2	2	600–1100	10–30	0.3
TWIP	1.5	20–35	4	4	500–700	50–90	0.5
DDG	0.05	0.4	0.05	–	250–350	25–35	0.2

nace. A steel shell solidifies around the cylinder under controlled conditions. After a period of 12 s, the lower part of the cylinder is moved downwards to a given total elongation at a controlled velocity. Force and elongation are recorded and the solidified specimen is subjected to metallographic examination. Cracks are counted and the total length of the cracks is measured.

Different solidification experiments were carried out in order to investigate segregation on the micro- and macroscopic levels. Extensive metallographic work and microprobe-analysis of cast and cast-and-rolled specimens permitted the validation of segregation calculations and the identification of the composition and size distribution of non-metallic inclusions.[9,10] The solidification range of the alloys was described based on data from DSC measurements and ThermoCalc(TC) calculations.[11] Scale formation under continuous casting conditions was investigated using a DTA in a water-vapour atmosphere up to 1300 °C.[4]

Solidification Analysis

It is well known that the formation of segregated internal cracks during the solidification of steels is related to the brittle temperature range between the LIT (liquid impenetrable temperature) and the ZDT (zero ductility temperature), ΔT_B. The LIT is associated with a solid fraction of 0.9 and the ZDT corresponds to a solid fraction between 0.98 and 1.[12] Several hot tearing criteria define a limiting critical strain which is a function of the steel composition and the strain rate. In general, a wider brittle temperature range results in a higher crack susceptibility. The higher thermal contraction immediately above or below the solidus temperature, caused by the δ-γ-transformation during the peritectic reaction,[13] also indicates higher crack susceptibility.[14]

Our analysis of the solidification using DSC measurements and TC calculations is therefore a first attempt to compare quantitatively the tendency for internal cracks to form in different steel grades.

Figure 1 compares the phase transformations during solidification of the selected steel grades (TCW3, steel database: TCFe3 TCS v.2), Table 2. The ULC steel and the electric strip steel both solidify as primary ferrite. The ULC steel grade behaves similarly to pure iron. The electric strip steel is free of transformation between the solidus and 1000 /C. The HSSS steel undergoes a peritectic transformation, whereas the X50MnAl 25 1 transforms to austenite and is free of further transformation between the solidus and 1000 °C.

Table 2 shows the composition of the four steel grades investigated and summarizes the TC calculations and the results of the DSC measurements for the X50MnAl 25 1. The calculated and measured liquidus and solidus temperatures correlate quite well.

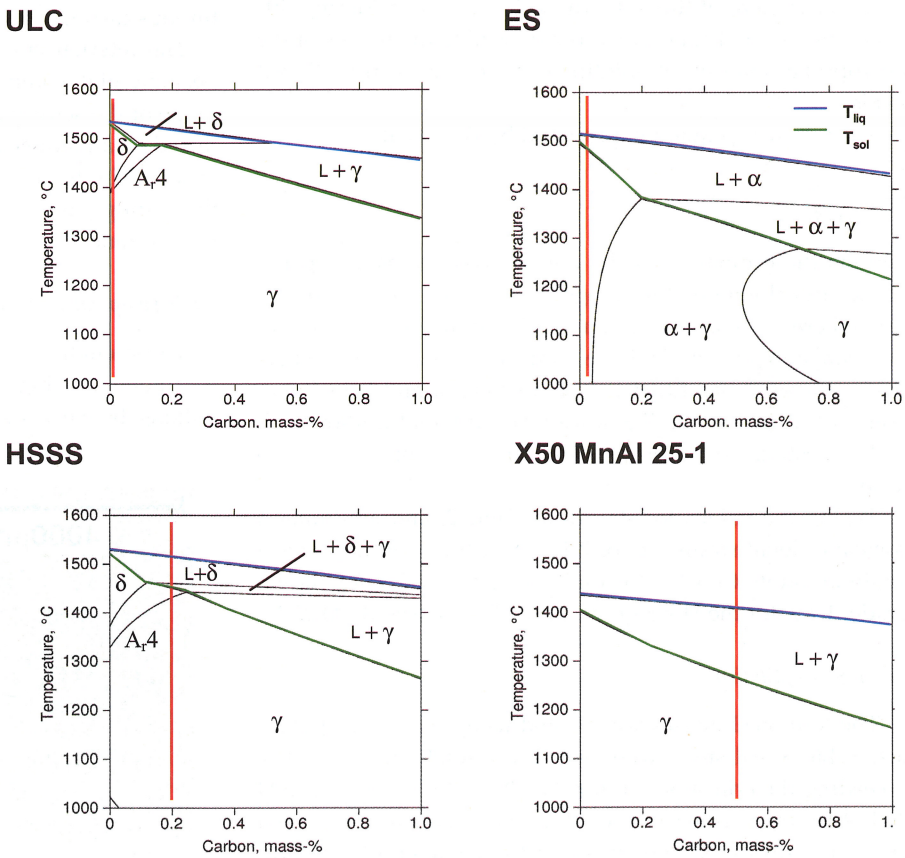

Fig. 1. Calculated phase systems from ThermoCalc (TCW3/TCFe3 TCS v.2).

Table 2. Composition of selected steel grades for ThermoCalc calculations and experiments, calculated temperatures from ThermoCalc (TCW3/TCFe3 TCS v.2), measured temperatures from DSC-analysis (cooling rate 2 K/min), ΔT_B: temperature range between solid fraction 0.9 and 1.0, δ-γ-transformation between solidus temperature and 50 K below solidus from ThermoCalc in %.

	ULC	ES	HSSS	X50MnAl 25 1
C, wt.-%	0.005	0.01	0.2	0.5
Mn, wt.-%	0,17	0.25	1.7	25
Al, wt.-%	0.04	1.0	–	1.0
T_L, °C (TCFe3)	1535	1511	1514	1411
T_S, °C (TCFe3)	1512	1489	1451	1289
T_L, °C (DSC)	–	–	–	1420
T_S, °C (DSC)	–	–	–	1305
ΔT_B, °C	5	5.5	25	171
δ-γ-transformation, %	0	0	25%	0

The calculation of ΔT_B requires the consideration of non-equilibrium conditions. A microsegregation calculation, here based on a modification of the model proposed by Ueshima et al.[15] yields ΔT_B values between 5 and 171 K. The calculated enrichment of the individual elements, considering diffusion in the solid state, corresponds well to the results of the microprobe analysis of solidified specimens of the alloyed steels.

The following equation, proposed by Won et al.[12]

$$\varepsilon_C = \frac{\varphi}{\Delta T_B^a \cdot \dot{\varepsilon}^b} \quad (1),$$

permits the estimation of the critical strain ε_C as a function of the critical temperature range ΔT_B and the strain rate ε, in 1/s, where is a constant and a and b are the brittle temperature range exponents and the strain rate sensitivity, respectively. Pierer[16] has fitted the parameters, a and b in Equation 1 to results in the literature from different authors[17–19] and has estimated values of 0.0107 for, 0.505 for a, and 0.305 for b.

Taking the values for ΔT_B from Table 2, and assuming a constant global strain rate of $2 \cdot 10^{-3}$ 1/s, the resulting critical strain amounts to 3.2 % for the ULC grade, 3.0 % for the ES grade, 1.4 % for the HSSS grade, and 0.5 % for X50MnAl 25 1.

Crack Susceptibility

The four steel grades were tested using the SSCT apparatus, Table 3. All steels were tested at a total strain of 2.0 %, exceeding the critical strain for the HSSS steel and X50MnAl 25 1. After the tensile test, the solidified specimens were taken out of the steel melt and subjected to metallographic examination. Figure 2 shows a micrograph with a primary etching

Table 3. Parameters for the SSCT-tests, t_H: holding time before loading, t_T: loading time, t_S: total solidification time, all in seconds.

	Parameters for SSCT tests
Cylinder	Low-alloyed steel, diameter 56 mm, height 50 mm
Cooling rate	uncoated surface, maximum heat flux 6-7 MW/m, mean heat flux 1.5-2 MW/m
t_H, t_T, t_S (s)	12/10/27
Strain rate (1/s)	$2 \cdot 10^{-3}$
Total strain	0.02, corresponding to 1 mm elongation

of the HSSS steel sample after straining at 2.0 %, and with a number of segregated internal cracks. Eight micrographs were prepared from every specimen and the total crack length, the mean crack length per specimen, and the number of cracks were measured. Figure 3 shows the mean internal crack length for the four tested steel grades. The ULC steel was found to be free of cracks and the ES steel was almost free of cracks. Cracks were found in the HSSS sample, and the X50MnAl 25 1 proved to be the most internal-crack-sensitive steel grade. The results are in good agreement with the theoretical considerations. In the case of the HSSS steel, the strain caused by contraction during the peritectic reaction is an additional reason for the higher crack sensitivity. Peritectic steels are generally well known as being very critical in continuous casting.[20]

The internal crack susceptibility of X50MnAl 25 1 is expectedly high compared to the low-carbon steels but is in the range of the sensitivity of higher carbon steels which are produced on an industrial scale. Nevertheless, defect-free casting of high-Mn, high-Al steels will require careful adjustment of the casting parameters in order to minimize the strain in the mushy zone.

High Temperature Strength

The strength of the cast material plays an important role in continuous casting: A higher resistance of the strand shell to bulging between the rolls of the casting machine decreases

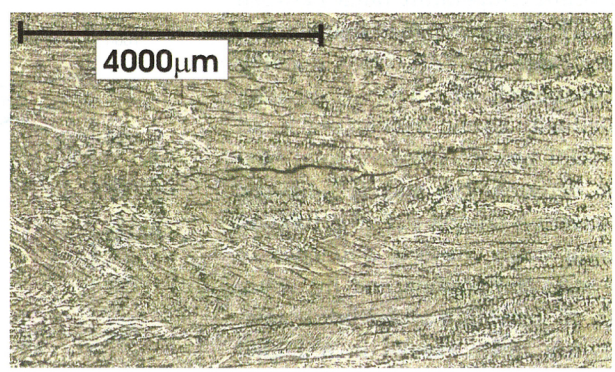

Fig. 2. Micrograph from specimen of steel grade HSSS with segregated internal cracks, etching Bêchet-Beaujard.

ADVANCED ENGINEERING MATERIALS

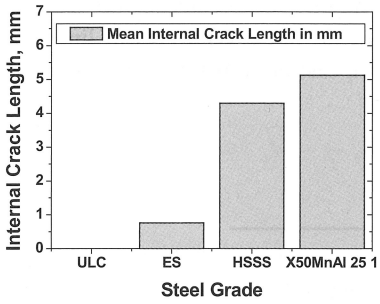

Fig. 3. Mean internal crack length per specimen in mm.

the tensile strain in the mushy zone and reduces the risk of internal crack formation. On the other hand, high-strength steels are also reported to develop deep oscillation marks,[21] which increases the risk of transverse- and corner-crack formation at the surface of the cast product. The strand guiding system, especially in the bending and straightening zone, has to absorb higher loads, and roll wear increases.

High-Mn steels reportedly have high strength at elevated temperatures. A review of the high-temperature strength data, as given in the literature, of different steels near the solidus temperature yields a fourfold higher strength for austenite compared to ferrite.[22] Results are rarely given for high-Mn steels. The extrapolation of results from hot tensile tests on steels with up to 5 % Mn[23,24] would suggest only a slight increase in tensile strength for higher-Mn steel compared to a common HSSS steel.

Figure 4 shows the force-elongation curves for the four previously described SSCT tests. For a better understanding of the results, it should be noted that the tensile test is performed on a strand shell after 12 sec. of solidification. The temperature gradient over the shell thickness depends on the existence of the various phases. In the case of the transformation-free steel grades, ES steel and X50MnAl 25 1, the shell consists only of either ferrite or austenite. In the case of the ULC and the HSSS steel grades, the part of the shell at a temperature below A_r4 (see Fig. 1) is austenitic. This increases the measured tensile strength remarkably.

As expected, the ferritic ES steel has the lowest tensile force and X50MnAl 25 1 the highest. In the case of the HSSS steel, partial crack formation in the shell reduces the sectional area of the solidifying specimen, resulting in a lower tensile force compared to the ULC steel.

For a better interpretation of the test results, a coupled thermal-mechanical model of the SSCT test has been developed.[25,26] Due to the constant global strain rate during the SSCT tests, a simple elasto-plastic approach is sufficient. The total strain $\varepsilon_{tot}(t)$ is split into an elastic term $\varepsilon_{el}(t)$ and an inelastic term $\varepsilon_{pl}(t)$.

$$\varepsilon_{tot}(t) = \varepsilon_{el}(t) + \varepsilon_{pl}(t) \quad (2).$$

Inserting Hooke's law for the elastic term and the Hollomon equation for the inelastic term, results in Equation 3:

$$\frac{\sigma(t)}{E} + \left(\frac{\sigma(t)}{K_P}\right)^{\frac{1}{n}} - \dot{\varepsilon} \cdot t = 0 \quad (3).$$

In order to calculate the time-dependent stress $\sigma(t)$, Equation 3 must be solved for every element and time step. E, K_P and n are temperature-dependent. The elastic modulus, E, was calculated using the relationship proposed by Kinoshita.[27] The strain-hardening exponent, n, which is assumed to be dependant on the strain rate, was determined from experimentally obtained curves related to the Zener-Hollomon parameter Z,[28] where Q denotes the activation energy.

$$Z = \dot{\varepsilon} \cdot \exp(Q/RT) \quad (4).$$

K_P, the plastic resistance, is temperature- and composition-dependant. To account for the thermal activation of the high-temperature plasticity, K_P is defined using a power law of the form

$$K_P = A \cdot T^m \quad (5).$$

The constant m is set to –4.283, A is used as a fitting parameter in order to adjust the calculated force-elongation curves to the measured ones, Table 4.

Figure 5 shows the calculated force-elongation curves for the four steel grades. In general, the difference between the

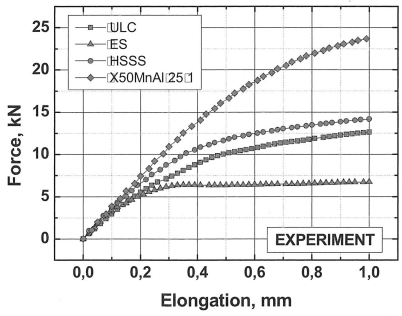

Fig. 4. Force-elongation curves for the four steel grades from SSCT test.

Table 4. Parameters for the calculation of force – elongation curves used in Equations 3–5, T in °C.

Steel Grade	A MPa
ULC	$1.4 \cdot 10^{14}$
EB	$1.3 \cdot 10^{14}$
HSSS	$3.1 \cdot 10^{14}$
X50MnAl 25 1	$3.5 \cdot 10^{14}$

$E\ (MPa) = 3.146.10^4 - 22.56 \cdot T + 1.38.10^{-3} \cdot T^2$

$Q\ (J/mol) = 2.1 \cdot 10^5$

$m = -4.2830$

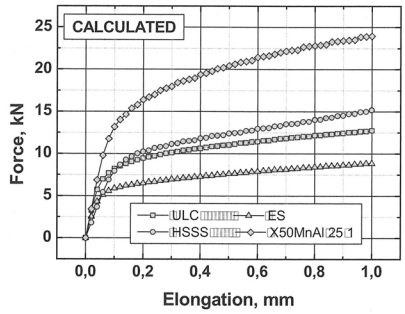

Fig. 5. Calculated force-elongation curves.

calculated and measured curves is highest for the initial slope. The reasons for this effect have been analyzed in detail in a previous paper,[25] and can be found in the relatively low stiffness and the geometrical characteristics of the testing arrangement, as well as in the commonly overestimated Young's modulus for temperatures near the solidus. The agreement between the measured and calculated tensile force is excellent.

Figure 6 summarizes the high temperature strength results for the four different steel grades. The strength has been calculated as the ratio of the maximum measured tensile force to the shell section area for a solid fraction of 1 at the corresponding solidification time. This is the strength of a solidifying strand shell after 24 sec of solidification. The relationships of the calculated strength values confirm the initial assumptions: high-Mn steels show a remarkably high high-temperature strength which is 4 to 5 times that of the low carbon steels, but only 1.5 times that of the common HSSS steel grade and in the range of that of high-C steel grades. The factor A in Equation 5 is only slightly different between the HSSS and the X50MnAl 25 1 steel, and, thus, the plastic resistance at the same temperature is similar.

Summary: the high temperature strength and internal crack susceptibility of a high Mn-steel grade, X50MnAl 25 1 has been compared to that of a HSSS steel and that of two low carbon steels. High strength and crack susceptibility are supposed to be limiting factors in casting high-Mn steels on conventional continuous casting machines. The actual results show, that crack sensitivity and strength are much higher compared to the low carbon steels, and also compared to the HSSS steel, but do not exceed critical limits of high carbon steels which are cast on industrial scale on conventional casting machines.

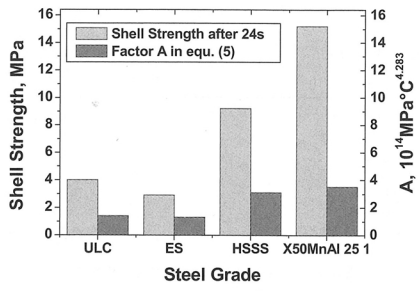

Fig. 6. Measured shell strength after 24s of solidification and factor A in Equation 5 for the four tested steel grades.

[1] O. Graessel, *PhD-thesis*, TU Clausthal, Germany, **2000**.
[2] G. Frommeyer, U. Brüx, P. Neumann, *ISIJ Int.* **2003**, 438.
[3] T. W. Kim, Y. G. Kim, *Mater. Sci. Eng.* **1993**, 13.
[4] G. Gigacher, *PhD-thesis*, MU Leoben, Austria, **2006**.
[5] G. Gigacher, C. Bernhard, W. Kriegner, *Forum for Metall. and Mater.* Leoben, Austria, May 27–28, **2003**.
[6] C. Bernhard, H. Hiebler, M. Wolf, *Trans. ISIJ* **1996**, *36*, 163.
[7] H. Hiebler, C. Bernhard, *Steel Res.* **1999**, *69*, 349.
[8] C. Bernhard, R. Pierer, A. Tubikanec, C. Chimani, *Continuous Casting and Hot Rolling Conf. (CCR04)*, Linz, Austria, June 14–15, **2004**.
[9] G. Gigacher, W. Krieger, P. R. Scheller, C. Thomser, *Steel Res. int.* **2005**, 644.
[10] G. Gigacher, *Prac. Metallogr., Spec. Ed.* **2004**, *36*, 51.
[11] G. Gigacher, *ThermoCalc User Group Meeting*, Aachen, Germany, June 24–25, **2005**.
[12] Y. M. Won, T. J. Yeo, D. J. Seol, K. H. Oh, *Met. Mater. Trans. B* **2000**, *31*, 779.
[13] A. Jablonka, K. Harste, S. Schwerdtfeger, *Steel Res.* **1991**, *62*, 24.
[14] C. Bernhard, G. Xia, *Ironmaking and Steelmaking* **2006**, *33*, 52.
[15] Y. Ueshima, S. Mizoguchi, T. Matsumiya, H. Kajioka, *Metall. Trans. B* **1986**, *17*, 845.
[16] R. Pierer, *Personal Commun.* **2006**.
[17] T. Matsumiya, M. Ito, H. Kajioka, S. Yamaguchi, Y. Nakamura, *Trans. ISIJ* **1986**, 540.
[18] J. Miyazaki, T. Mori, K. Narita, *Sec. Process Technol. Conf.* Chicago, USA, February 23–25, **1981**.
[19] K. Wünnenberg, R. Flender, *Iron and Steelmaking* **1985**, *12*, 22.
[20] M. Wolf, *Iron- and Steel Soc.* Warrendale, USA, **1997**.
[21] Y. Sugitani, M. Nakamura, *Tetsu-to-Hagane* **1979**, *65*, 1702.
[22] H. Mizukami, A. Yamanaka, T. Watanabe, *ISIJ Int.* **2002**, *42*, 964.
[23] H. G. Suzuki, *PhD.-thesis*, Tohoku University, Japan, **1981**.
[24] P. J. Wray, M. F. Holmes, *Met. Trans. A* **1975**, 1189.
[25] R. Pierer, C. Bernhard, C. Chimani, *Berg- und Huett. Monatshefte* **2005**, *150*, 163.
[26] R. Pierer, C. Bernhard, C. Chimani, "*Comput. Meth. and Exp. Measurements XII*", Malta, **2005**, 757.
[27] K. Kinoshita, T. Emi, M. Kasai, *Tetsu-to-Hagane* **1979**, *65*, 2022.
[28] M. Uehara, I. V. Samarasekera, K. J. Brimacombe, *Ironmaking and Steelmaking* **1986**, *3*, 138.

